Towards Parallel Bacterial Motion Detection

D.J. Degeling

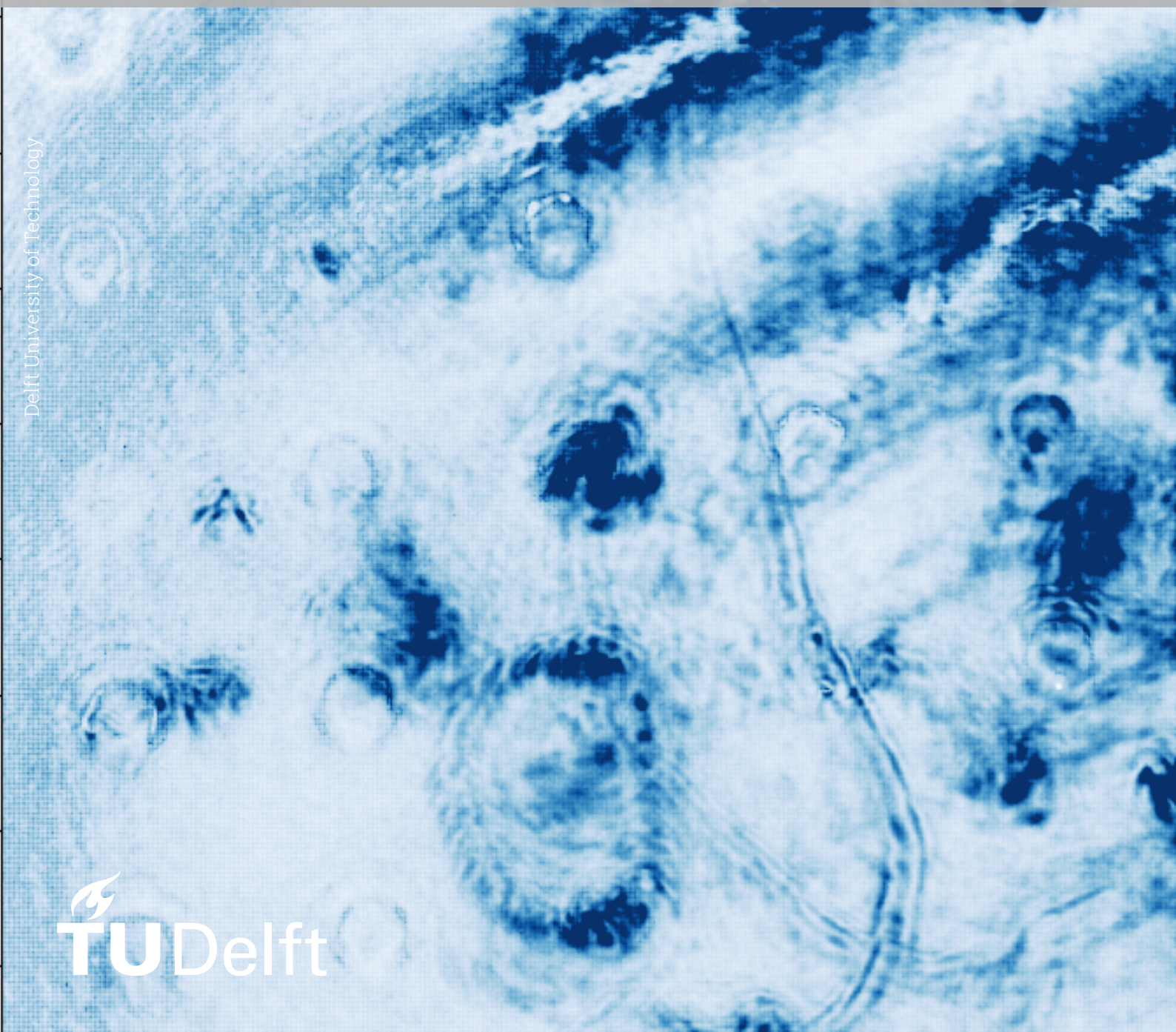

Delft University of Technology

TU Delft

Towards Parallel Bacterial Motion Detection

by

D.J. Degeling

Student Number 5137845

To obtain the degree "*Bachelor of Physics*".

Main Supervisor:	Prof. Dr. P. G. Steeneken
Daily Supervisor:	Dr. I. E. Roslon
Project Duration:	November, 2023 - February, 2024
Faculty:	Faculty of Applied Sciences

Cover: Heatmap of variance over pixel intensity, taken from a 30-minute measurement of a 5 by 5 grid of graphene membranes on which bacteria are deposited.

TU Delft

Preface

It has been very interesting to get an idea of what doing research is like, especially when being quite free in doing so. For this project, I am lucky to have been brought into contact with a startup which works on developing new AST techniques, SoundCell. The company revolves around a group of researchers who have made very interesting results in probing bacterial nanomotion over the last years. To get a feeling of what a startup can be like during this project, has been inspiring.

Having nice people around makes it even better, and for that I must thank all people involved around SoundCell. Especially E. Kingma, I. Roslon and S. Japaridze, all three always have been very helpful and were never bothered by the many questions I have been asking regarding their unique research. My supervisor P.G. Steeneken I want to thank very much for making it all possible and all the helpful advice throughout the project.

My housemates C. van Mierlo and S. Ruis I can thank for the usual gezelligheid, and their interest for my project has been appreciated a lot.

Dirk-Jan Degeling
Delft, February 2024

Abstract

One way to tackle the rise in antibiotic resistance, is to develop new techniques for testing the susceptibility of cells to antibiotics. In this paper, a comparison is made between a novel bacterial susceptibility testing method and a modification on this method. Both methods rely on bacterial samples deposited on graphene cavities, where the bacteria will stick to the graphene by the addition of APTES. By making use of a 632.8 nm He-Ne laser, the sample is probed, and the cavities then serve as ultrasenstive sensors for determining bacterial nanomotion. The existing method (single spot readout) is based on focusing a laser on graphene drums, where the drums are read out one at a time by the use of a photodiode. The modified method (parallel readout) makes, by the addition of one lens, use of an expanded laser, and a CMOS camera. At 100 frames per second, four drums are read out simultaneously. This technique hypothetically makes very high throughput possible for antimicrobial testing.

Both methods rely on converting a signal based on the intensity of the incoming light to the membrane deflection in nanometer, and the bacterial motility is found by taking the variance. The comparison of the two methods is done by performing multiple experiments, in order to relate the quality of the signal by finding the standard deviation (noted as S) of the variance of the deflection σ_z^2.

From an analysis of S, statistical quantities describing the distances between probability distributions have been conceived, and a criterion is proposed to differentiate between the noise levels of the two techniques. One such quantity is the normalized distance between the signals of two types of experiments, the one being an experiment without bacteria as a reference and the other being an experiment with living bacteria.

In the case of hypermotile bacteria, parallel readout has an average variance of deflection of $5.95\,\text{nm}^2$, it is substantially higher than the method of single spot readout, having average $2.92\,\text{nm}^2$. The unitless metric D for the distance between two signals however shows that both methods score similarly in probing nonmotile (Δ-MotAB) E. Coli, as for the parallel readout the measure has for Δ-MotAB a value 0.34 and for single spot readout it has the value 0.31. In the case of hypermotile (7740) E. Coli, parallel readout scores again better with a value of 2.35 versus 0.39, which is the value obtained for single spot readout.

Finally an outlook is given where interesting findings have been summarized. With the use of power spectral densities and heatmaps of either average intensity or variance of the signal, interesting phenomena are noted and are topics for future research.

Contents

1 Introduction

There is a worldwide rise in antibiotic resistance, and new methods for Antibiotic Susceptibility Testing (AST) may prove successful in bringing these worrisome developments to a halt. One new development is the use of bacterial nanomotion for AST[9] . The main idea of this new technique is to probe a sample of bacteria by making use of a very sensitive mechanical resonator that is read out optically. The use of an ultrathin graphene membrane as a mechanical sensor, makes it possible to detect motion on the scale of nanometers.

Methods that are specifically aimed at probing bacterial nanomotion, are a relatively recent development. This is because previously, the difficulties in probing (living) bacteria have been too great to overcome - this is partly because regular probing methods rely, in one way or another, on invasive processes. And it is these invasive processes which often lead to either bacterial death, or whose resulting signals have too small amplitudes and high levels of noise[10]. However, using invasive probing mechanisms has been necessary, because at the nanoscale, microscopes are limited. The limits follow from the nature of light itself, as visible light has wavelengths on the scale of hundreds of nanometers, and this poses issues rendering a *regular* microscopic setup in principle useless, concerning nanomotion detection.

Gaining insights into the nanomotion of bacteria has other applications besides determining the effects of antibiotics. It is also possible to explore into the inner workings of living bacteria[9]: by making use of selective antibiotics, which block only certain mechanisms of a bacterium, the nanomotion of a bacterium can, to some degree, be broken down to its constituent parts. In developing this new technique for nanomotion detection, one key step to be made is changing from single spot readout towards parallel readout. Single spot readout is the method currently used for probing bacteria where the individual drums are measured one-by-one using a laser and a photodiode. The parallel beam technique is to make use of an expanded laser and a CMOS camera to obtain data from a great range of wells simultaneously. This gives the AST technique much higher throughput, making it faster and more reliable due to higher sampling.

This paper is aimed at the development of this new technique, and specifically at comparing the noise sources that play a role in acquiring a signal from the CMOS camera. This will then be related to the current technique of single spot readout, where the laser is focused. There is currently no clear view yet of the noise inherently present in this new method, and whether it is beneficial at all to use, for example, the expanded laser.Nontrivial difficulties arise due to the wave nature of light and the limits of the sensors. The approach of the research in this report will be two-sided: on the one hand, we undergo a series of measurements for both methods, to yield a ratio of signal to noise. On the other hand, a more qualitative analysis of multiple aspects of the noise will be undertaken, in order to gain more insights into the causes of some noise sources.

After reviewing the literature on this topic in Chapter 2, both the experimental method and method for data analysis are presented in Chapter 3. This is then more clarified in Chapter 4, where a dive is taken into the optical characteristics of the set-up, and from this, the equation for membrane deflection, from which bacterial nanomotion is deduced. Then, Chapters 5 and 6 are aimed at further characterizing the two methods, part by theoretical speculation and part by a qualitative discussion by use of, for example, heatmaps, histograms or power spectral densities, all of which can serve as powerful tools to analyse the noise on a more fundamental level. Chapter 7 presents the results of the quantitative analysis by which the two methods can be compared. By having gradually added possible causes for noise in the measurements, we may be able to quantify their effect on the final signal. After these analyses, Chapter 8 can serves a recommendation - here, some possible strategies for reducing noise or enhancing signal quality are proposed. The report is then finalized in Chapter 9, where the conclusion states the benefits of using Parallel Readout compared to Single Spot Readout.

2 Literature Review

Before continuing towards the theoretical framework, it is wise to have a look into the previous works in the field. While much research is being done, there are still a lot of unknowns, and many methods which at the moment might seem irrelevant can come back into relevance as improvements may follow in the future. Starting with the conventional methods for AST, the following sections work towards new developments and the use of nanomechanical resonators.

2.1. The problem of rising resistance

Already in the 1920s, Alexander Fleming has developed the first method of testing bacterial susceptibility to antibiotics . Fleming is well known for his development of penicillin (1928), being one of the first widely used antibiotics. But as the use of antibiotics have grown tremendously from its invention onwards, the resistance of bacteria have increased as well[1]. Around the 1960s, this was being recognized and health instances start spreading awareness on good practice when it comes to administering antibiotics. More recently, in 2015 there is a Global Action Plan set up by the World Health Organisation to tackle antimicrobial resistance globally[6]. One of the key points is to develop knowledge on microbial resistance and push the development new methods related to AST.

2.2. Antibiotic Prescription

When, for example, a sick person is infected with a bacteria, a health professional can decide to prescribe a certain type of antibiotic drugs. The ways in which the professional decides the right drug to prescribe, can be divided into two categories. The most common being Empiric Therapy, where the professional takes all the patients' symptoms into account, as well as the location of infection, and deduces the most probable bacteria or bacterial group that could be the cause. Direct Therapy, on the other hand is less common. This is based on the exact knowledge of which bacteria is causing the infection, and ultimately, to which antibiotics the cell in question is most sensitive. This form of therapy is obviously much more efficient and leads to the least accumulation of bacterial resistance. The following section describes the Direct Therapy-methods available for describing the right antibiotic.

2.3. Antibiotic Susceptibility Testing methods

The standard methods of AST necessary to perform Directed Therapy, can be split up in a phenotypical and a genotypical category. The first one being based on the observable characteristics of a (group of) bacteria, and the latter on all genes present in the cells genome.

2.3.1. Phenotypic AST

Phenotype-based susceptibility testing is a robust and intuitive way of telling apart the effects of certain antibiotics. The working principle is that bacteria can be grown over time in a broth, which is a nutrient rich medium in which bacteria, if let by itself, thrive. Then, on a Petri dish multiple cultures of bacteria are separated and administered different drugs, and a control group is set apart as well. After a certain amount of time, which could range from several hours up to a day, the cultures are inspected and it can be decided which antibiotic served most based on the cultures' growth patterns.

Here, it is important to have each cell culture start on equal ground, that is to say, each sample should have the sample density of cells. The metric relating this aspect of a cell culture is O.D.600, meaning the optical density of cells measured with light having wavelength $600\,\text{nm}$.

2.3.2. Genotypic AST

PCR testing specifically for determining antibiotic susceptibility. These methods however are expensive and labour intensive, while at the same time the resistance is indirectly deduced from the presence or absence of certain genes. Even then, the conclusion can be incorrect due to some of these genes not being phenotypic.

2.4. Contemporary methods

From around the year 2000 and onwards, many initiatives have been undertaken within the scientific community to seek for new methods which deter-

mine antimicrobial sensitivity. As summarized by Pujal-Vila et al.[7], many of these methods rely on the principles of Atomic Force Microscopy (AFM). In AFM, a cantilever tip is used to probe surfaces and the relevant atomic forces cause the tip to bend and this in turn yields a signal. Scanning an entire surface, the signals combined yield what is known as a topography. However, for sensing bacteria, the AFM is used in a nontrivial manner: a certain amount of cells are adhered onto the cantilever, and then the movements of this colony induces a signal of interest.
Based on this, many variants of AFM-based AST methods have been attempted and further developed. By either varying the adhesive medium, the specific cantilever or the bacterial colony characteristics, methods have been successfully developed to probe nanomotion. The following figure places these new methods into context with the regular AST methods, and from this it is clear that there are enormous benefits to methods based on nanomechanical sensors.

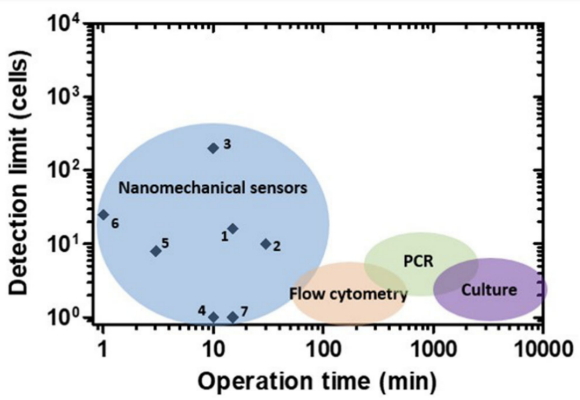

Figure 2.1: ”Performance of nanomechanical sensors for bacteria detection” [7]. [Nanomechanical sensors show promising results for short operation times, although the detection limit can be somewhat lacking. The figure makes the comparison with some of the most widespread conventional methods”].

2.4.1. Graphene based nanomechanical sensor

The method researched for this report makes use of an array consisting of graphene membranes, onto which individual bacteria are adhered. The novelty of this approach is to choose for an nanomechanical sensor not based on a variant of an AFM, but instead takes the bacteria on chip which is scalable and in which bacteria can be read out individually.

2.4.2. Graphene characteristics

Graphene is a material that exists of single layer of carbon atoms, formed in a hexagonal pattern. It is a very novel material, because it has been first produced and identified in 2004[3], and since then countless of research has been done to understand and utilize the unique properties this material has. One such initiative, is the founding of Graphene Flagship[15], which is an European Union-wide research initiative that aims for more collaboration, with over 100 research oriented companies involved.

2.4.3. AST future perspectives

Both the ever continuing rise in antimicrobial resistance, and the wish for further improvements in personal healthcare, call for further developments in AST. As the currently studied nanomechanical sensors further develop, they may play a significant role in improving AST.
Such improvements could be for instance, the application of a machine learning model[12], trained specifically at recognizing a bacterium and its state. Another such improvement could be by an enhancement of signal stability[7], as the signal of a nanomechanical device is obviously very sensitive to external noise sources and thermal drift.
Finally, parallelization of the readout technique can pose multiple benefits as well for the development of AST[10]. in this case, parallelisation means the modification of the AST technique in such a way that multiple bacteria are probed simultaneously, leading to a higher throughput, decrease in duration and possibly a increase in reliability due to higher amount of testing. By scanning multiple cavities simultaneously, the effective cost per analysis can even be reduced, possibly drastically, as the number of simultaneously scanned cavities might grow to hundreds or thousands. However, before being able to make these leaps in magnitude, certain drawbacks need to be overcome first. In general, the components of a set-up meant for discrete analysis lack scalability and also For the future of AST[7], prototype fabrication, decrease of noise sources.

2.5. Research statement

As one of the perspectives for improvements of AST revolves about the development of parallelisation of the readout, this makes an interesting topic of study. As of yet it is unknown in what form and whether at all parallel readout membrane arrays is possible for AST using the current techniques. In this regard, Pujal-Vila et al. (2020) states the following about the status of parallelisation of AST: ”The poor scalability [...] has limited the number of sensors measured simultaneously (below 10

sensors)", stating the current status.
This research is aimed to investigate the use of parallel readout of graphene membrane arrays. The main question of this investigation can be phrased as:

"Are the signals obtained from parallel readout of graphene arrays, by the use of an expanded laser and CMOS camera, suitable for measuring bacterial nanomotion?"

3
Experimental set-up and method

This chapter aims to give a combined presentation of the set-up and the method by which the nanomotion experiments have been conducted. The main principle of the experiments is to have bacteria on top of cavities which are covered by graphene layers. These instruments are referred to as drums. Such a drum then forms an ultrasensitive device from which bacterial motion can be deduced. However, as this report aims to compare an established version of the method to a novel alternative, it is good to note that for the description of this new method, that it will likely be subject to change in the future.

The following method is for experiments where motion of (several types of) E. Coli bacteria can be measured on the nanoscale, possibly when exposed to antibiotics. In this case, use is made of a graphene membrane over multiple cavities. We start by describing how a bacterial colony is grown and put in place, followed by an overview of the set-up and it's use, after which possible options for data analysis will be discussed. This chapter is concluded by a list of specific experiments conducted for this research, meant for comparing noise levels in the method of Single Spot Readout versus that of Parallel Readout.

3.1. Experimental Procedure

The preparation for the experiments have been done a day before the measurements. Because the day before, the dedicated strain of E. Coli is selected, and grown overnight in LB (Luria-Bertani) growth medium at 37 °C . On the day of the experiments, this suspension should be checked for Optical Density (OD), and diluted until the OD is around 0.2 . Because these measurements are aimed at obtaining nanomotion, APTES is added to the bacterial suspension, such that a final concentration of 0.05 - 0.1 % is reached. Too much will have a negative effect on the bacteria.

The laser should be turned on already about one hour before starting measurements, to reduce this possible source of signal drift. The collected graphene chips should first be cleaned using a gas pocket pump, and attached to the bottom of a fluidic chamber with double sided tape. For these measurements, a FCS3 circular flow chamber has been used, and after the flow basket has been reinstalled with glass lid, the basket was tightened under the microscope objective. The flow basket is connected on two sides with tubes for an in- and outlet of fluids, which are controlled by a high accuracy microfluidic pump. This is used to control the flow and flush of bacteria onto the sensors.

3.2. Set-up Overview

A schematic of the set-up is shown in Figure 3.1, as is used in the method of Single Spot Readout.

3.2.1. Calibration

The experimental procedure further takes a few manual alignment and calibration steps. One such step is to achieve the right height for the sample, such that it is in the focal spot of the set-up. Since the device is very sensitive, this can change under certain conditions, and after bringing it close to the focal plane by hand it should be further adjusted via the computer using the remote controllers for height.
Furthermore, the reflected laser power should be calibrated for as well. By adjusting the neutral density filter that is in front of the sample, a measured Power of 0.8V or 1.0 V was set for Single Spot Readout and Parallel Readout, respectively.
Also, the pressure from the microfluidic pump is set by hand, while at the same time looking at the results on a screen from the microscope. Once a certain stage is reached, the pump can be stopped. For example, when flushing in bacteria, one should wait for the bacteria to be mostly attached onto the graphene, and when flushing out, one should wait for most of the bacteria to be removed. After finishing the experiments, the chamber must be flushed with ethanol to kill re-

maining cells, and in case of pathogenic cells there must be further sterilisation of the under a UV lamp overnight.

3.2.2. Laser properties

For both readout methods, a Helium-Neon laser was used. This device emits light based on the atomic transitions in a gas, and emits light at a wavelength of $632.8\,\text{nm}$ (in air), and can be regarded monochromatic. After making an angle due to a mirror, the beam is expanded by a pair for lenses and then the polarization is altered by a $\lambda/4$ plate. After returning from the sample, light gets split by the two polarized beam splitters such that the photodiode and camera both obtain part of the intensity that is reflected.

In the case of using the method of Parallel Readout, this schematic is altered by a single added lens. This lens is placed before the objective, in such a way that their focal points overlap and the light that comes out of the objective is collimated. In this way, the laser shines on an expanded area, and multiple drums reflect at the same time back towards the CMOS camera.

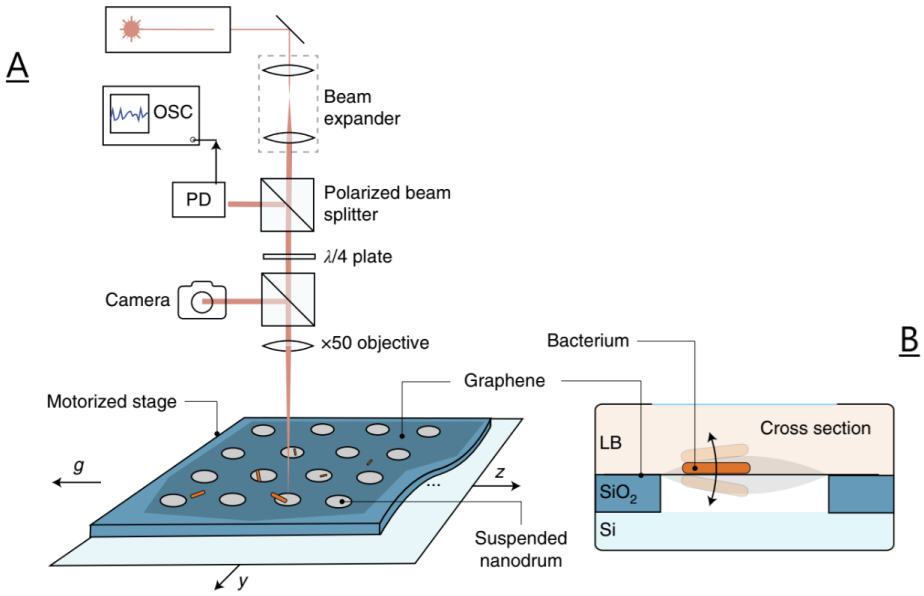

Figure 3.1: A: Experimetal set-up as used in the method of Single Spot Readout. B: A cross-section of a drum on which a bacterium is deposited. OSC and PD stand for oscilloscope and photodiode, respectively. Image adopted from Roslon et al. (2022)[9]

3.2.3. Camera properties

For Parallel Readout, a Thorlabs CS235CU CMOS camera[13] has been implemented into the set-up for data acquisition, and combined with the Thorcam software, this has been used to obtain high quality, uncompressed stacks of images (of type TIF), of which the time interval is set in advance. The camera has an ADC (analog-to-digital-converter) of 12 bits. That is to say, it has $2^12 = 4096$ discrete levels to store information of incoming light intensity.

As seen in part B of Figure 3.1, the chip consists of a silicon substrate on which a layer of SiO_2 is deposited, and in which holes have been formed. These holes form the cavities which, in combination with the layer of graphene on top, act as nanomechanical resonator, or more intuitively, drums. The cavities used in these experiments have a radius of $10\,\mu\text{m}$ and a depth of $285\,\text{nm}$. On top of the cavity is a bilayer of graphene, covering the entire chip. For probing nanomotion, use has been made of APTES, and then a bacterium becomes stuck on the graphene. In the case it ends up on a cavity, it can be probed very sensitively due to the optical properties of the drum. In the following chapter, the theory regarding this optical system will be presented.

3.3. Method for signal analysis

In the case of Single Spot Readout, the photodiode obtains the signal and a script automates the horizontal placement of the sample, for which parameters can be set initially. These parameters are: the timelength of one datatrace (set for 30s), the amount of rows and columns of drums to be probed and the initial location and the location of the opposite corner for skewness correction. This automated script also has control over the microcontrollers, such that after each measurement, the sample is relocated and a next drum in the predefined array is probed by the laser.
From this we obtain arrays containing timestamps and the measured voltage at the photodiode, V_{pd}. Using a conversion from voltage to deflection $z(t)$, which will be derived in the following chapter, a ballpark estimation can be made for the amplitude of motion of the bacteria.

For parallel readout, the image format is TIF. This uncompressed format has been chosen, because for high resolution signal analysis, compression could mean loss of crucial information. Knowing the interval between each image in advance, a video can be reconstructed. The FPS (frames per second) has been set for all measurements to 100, and each has a time length of 30 seconds. However, for this method, there is no automated script yet and the positioning and executing of measurements have been done by hand. To analyse the TIFF files, I chose to work by scripting in Python, and here I made use of the *tifffile* package for importing the data. Using this, a 4-D array can be imported with the following axes: time, x-pixel-coordinate, y-pixel-coordinate, and color code. For example: data[400][100][100][0] results the intensity at timestamp 400, location (100,100) for the color red (0). The data is relatively big, each measurement taking over 1 Gigabyte. Here I chose to create a so called mask on the image, where I only took values near a predefined location of interest. This region was meant to have the same area as a focused beam, that is $4\,\mu$m[8], where a calibration from pixels to micrometers can be achieved by taking the cavities, being $8\,\mu$m, as a reference.

3.4. Conducted experiments

The goal is to gain insight in the baseline noise levels for Parallel Readout and Single Spot Readout, thus experiments have been conducted in such a way that possible noise sources are added one-by-one. To gain further understanding of the signal buildup, measurements have been done (1) with only air and (2) with only pure LB without any cells, and after this, (3,4) two types of E. Coli have been introduced to the LB to do nanomotion measurements on these. The measurements on air and LB then serve as a reference signal, and it is expected the noise levels in LB are higher than in air, possibly due to fluid flow, optical properties of the broth and Brownian motion of the particles wihtin it.

The two types of cells that measurements will be done on are two strains of E. Coli, with the phenotypic difference being that the one is hypermotile the other is non motile (Δ-MotAB). The hypermotile E. Coli has more flagella, and Δ-MotAB has a specific gene deleted such that it cannot move, as its motors are disabled.

Also, it has been chosen to not only take measurements from the surface of the cavities, but also in the region around them (around $2\,\mu$m to $4\,\mu$m away from two to four drums), and more far beyond (over $16\,\mu$m away from nearest drum). In figure 3.3 a schematic is shown with all the options. As can be seen there, a distinction is made between three possible locations for measuring. These three locations are shown in figure 3.2 as well. The hypothesis is that near the cavity, diffraction from the cavities can cause an increased level of noise around them, such that the location near a cavity will have increased signals, and far from the cavity will be the least noisy and could be regarded as a reference signal.

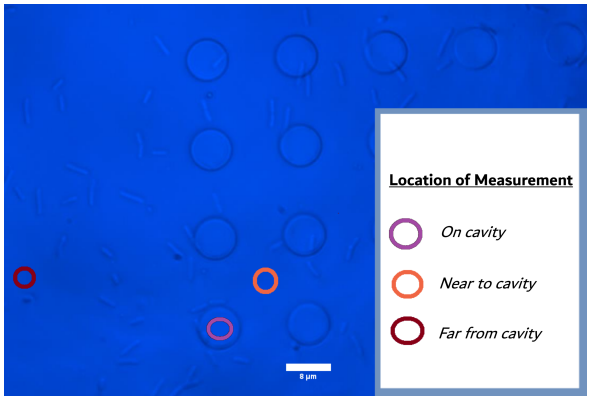

Figure 3.2: Image taken during the bacterial measurements. The laser is not turned on at the moment, and a blue light is shined on the chip. This part of the image is at the border of the array of drums that have been measured on, showing the region far from cavities.

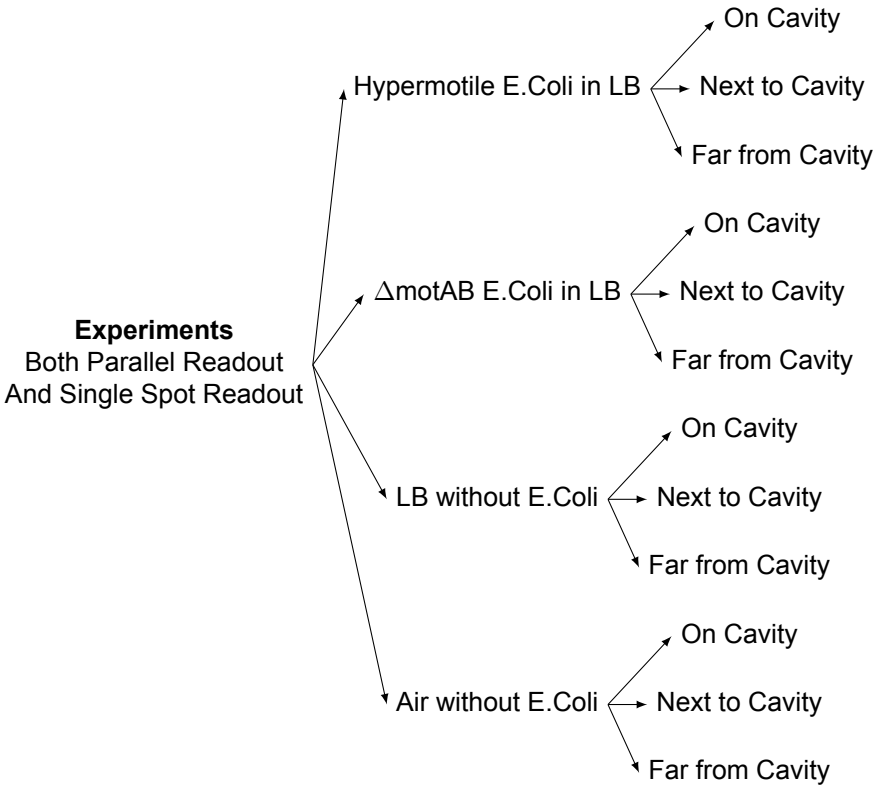

Figure 3.3: A tree schematic showing the relation between the 12 conducted experiments by relating each of the three probing locations to each of the four media.

4
Theoretical Framework

Now that the experimental set-up has been discussed, it is enlightening to dive into the underlying theory. After placing the need for better resolution in a theoretical context, this Chapter will continue on some basic working towards a basic understanding of related optics, finally towards the principles that make the probing of nanomotion possible, particularly, the ultrasensitive nature of Fabry-Pérot interferometers. One goal of this chapter is to give a derivation of the equation of membrane deflection. This equation makes possible the conversion of either photodiode voltage or pixel intensity to bacterial nanomotion, depending on the method used. The second halve of this chapter is dedicated to signal analysis-related theory, on which our analysis of noise for the two methods is built.

4.1. Cell motion at nanoscale

Typically, a bacterium moves by tumbling in random walks. This means that its entire body is rolling over the surface on which it is deposited, all stochastically. It does so in such a manner that on average it ends up at the same place it started. This means that although is has a significant speed of multiple microns per second, that on average, over time, it hardly moves as it gets back to initial position. When there is some form of attractor, such as a osmotic gradient which could be a hint for food or simply a better environment, the bacterium tends to move at this direction and it cannot be considered a random walk anymore.

By the use of (3-Aminopropyl)triethoxysilane (APTES) at the concentration given in Chapter 3, the bacteria become stuck on the graphene surface. If the APTES is too concentrated or has become oxygenated, it could lead to unwanted effects such as bacterial death. Other than that, APTES is a suitable chemical for sticking bacteria.

4.2. Microscopic limit

A micrometer consists of 1000 nanometers, and since a bacterium is sized typically in the order of $1\,\mu$m-$10\,\mu$m, it is good to realise this technique is inherently different from the usual probing by microscope. Under a microscope one can already probe a bacteria, and from that point it needs further explanation why there is a need for better imaging.

The key thing here, is that the motion of bacteria can be at the scale multiple microns, which is thus visible by eye. This is because a bacteria uses its body to tumble around, and can traveled distances that exceeds its body length by many multiples in a few seconds. On the other hand, when, for whatever reason, a bacteria is immobilized due to hunger or a missing flagellum, by eye it seems to sit still in place. But such an immobilized cell does, in fact, still have motion, but it is not clearly visible anymore using a microscope. In that sense, the regular probing by microscope has reached it's limit.

There are multiple metrics for the limits on optical system, one such being Abbe's Diffraction limit for microscopes. This limit quantifies the minimum resolvable distance, that is the smallest length a visual detail can have from an optical system. The limit is based on a concept and dimensionless number known as Numerical Aperture (NA). The number represents the amount of light a microscopical system can pick up, and is calculated using the half-angle made a cone of rays going from, say, the sample to the objective. The following formula gives the Numerical Aperture based on the half-angle θ and the index of refraction n of the medium the lens is in.

$$\text{NA} = n\sin(\theta)$$

The Abbe Diffraction Limit is a measure of the smallest object d that can be visualized by a microscope based on the relation:

$$d = \frac{\lambda}{2n \sin\theta} = \frac{\lambda}{2\text{NA}} \tag{4.1}$$

Here, λ is the wavelength, often given in nanometers, leading to a minimum resolvable distance expressed in nanometer as well. This distance is in the x-y plane and can be viewed as the minimum diameter of distance in the focal plane that is necessary for two details to appear distinct to the human eye. Even mor eimportant than the smalle

4.3. Membrane reflectivity

We can relate the voltage given by the photodiode V_{pd} to the intensity emitted by the laser I_0, by making use of the reflectivity of the sample R, which is a function of graphene membrane deflection z.

$$V_{pd} = \alpha\, R(z) I_0$$

Of crucial importance is the fact that the reflectivity depends on the deflection of the membrane, making movements modulate the light. This paragraph is meant to find the reflectivity $R(z)$, in order for the following paragraph to end up at an equation of membrane deflection as a function of read out photodiode voltage: $z(V_{pd})$.

4.3.1. Fresnel Coefficients

An interface is a border where to different media of differing refractive media come together, and here boundary conditions apply Maxwell's equations of the electric and magnetic fields. From these boundary conditions follow the Fresnel coefficients, which describe the behaviour of light at these interfaces. Although light is polarised in two directions, for this digression, one such direction will suffice and hence we will deal with only one coefficient for reflection and transmission.

$$r_s = \frac{n_1 \cos(\theta_i) - n_2 \cos(\theta_t)}{n_1 \cos(\theta_i) + n_2 \cos(\theta_t)}$$
$$t_s = \frac{2n_1 \cos(\theta_i)}{n_1 \cos(\theta_i) + n_2 \cos(\theta_t)}$$

These equations represent the Fresnel reflection and transmission coefficients for s-polarized light, and will be of use later in the derivation for membrane deflection.

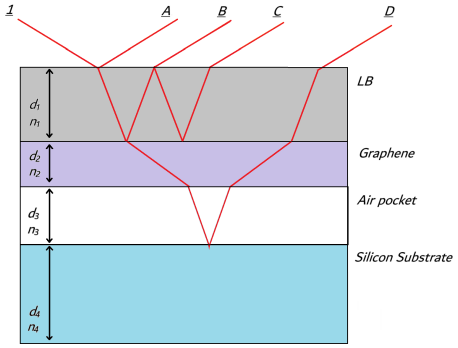

Figure 4.1: Stack of thin layers, with indices of refraction n_i and thicknesses d_i. Some possible paths are indicated. Image created by the author, but inspired from Leracuyer[4].

4.3.2. Stack of multiple thin films

Here we work towards the dependence of the reflected light intensity on the position of the graphene membrane. The cavity can be regarded as a stack of different materials, each of which has its own index of refraction. For this combination, light can travel in such a way that it oscillates up an down multiple times before leaving the cavity. To gain insight into the properties of such a device, P. Rouard established a method to do calculations on a stack of thin layers. In the following we adopt an extended version of the method of Rouard, by A. Vasicek[14].

Looking at Figure 4.1, we can start considering the stack of multiple thin layers one by a time, as is done by Leracuyer et al.[4]. Taking the incoming ray normalized, the first reflected ray as depicted by A, is then equal to the Fresnel coefficient for reflection of the first layer, r_{0-1} . Going towards the second reflected ray, B, it can be seen that this ray has taken an additional path towards the boundary of layers 1 and 2. It attains additional phase factors for each time it traverses this first stack, which all adds up to:

$$\underline{\mathbf{B}}: \quad r_{0-1} = t_{0-1} e^{-i\delta_1} r_{1-2} e^{-i\delta_1} t_{1_0}$$

Where the phase factors $e^{-i\delta_i}$ depend on the index of refraction n_i , traversed path $d_i cos(\theta_k)$ and wavelength of the used light λ :

$$\delta_i = 2\pi \frac{n_i d_i}{\lambda} cos(\theta_k) \tag{4.2}$$

Next, the ray denoted by C can be found as follows:

$$\underline{\mathbf{C}}: \quad t_{0-1} e^{-i\delta_1} r_{1-2} e^{-i\delta_1} r_{1-0} e^{-i\delta_1} r_{1-2} e^{-i\delta_1} t_{1-0}$$

Which can be rewritten as

$$\underline{\mathbf{C}}: \quad t_{0-1}t_{1-0}e^{-i4\delta_1}r_{1-2}^2r_{1-0}$$

From this we can see that all the rays that come from the bouncing within this first layer, can be contributed as an infinite sum[4]:

$$r_{1-2} + t_{1-2}e^{-i\delta_2}r_{2-3}e^{-i\delta_2}t_{2-1} + t_{1-2}e^{i\delta_2}r_{2-1} \times e^{-i\delta_2}r_{2-3}e^{-i\delta_2}t_{2-1} + \dots$$

This can be summed very neatly, as it forms a geometric series:

$$\sum_{n=0}^{\infty} ar^n = \frac{a}{1-r}$$

For which the convergence holds if $r < 1$. Our series has common term $(e^{-2i\delta_2}r_{1-2}r_{2-3})$ which is raised a power with each following entry. Thus all the rays bouncing from the first layer can rewritten as:

$$\begin{aligned} r_2 &= r_{1-2} + \sum_{n=0}^{\infty}(e^{-2i\delta_2}r_{1-2}) \\ &= r_{1-2} + \frac{t_{1-2}r_{2-3}t_{2-1}e^{-i\delta_2}}{1-(e^{-2i\delta_2}r_{1-2}r_{2-3})} \end{aligned} \tag{4.3}$$

We can generalise this equation using the following equality following from the Fresnel equations[4]:

$$t_{1-2}t_{2-1} = 1 - r_{1-2}^2 \tag{4.4}$$

Substituting this in the equation for r_2 yields:

$$r_2 = \frac{r_{1-2} + r_3e^{-i2\delta_2}}{1 + r_{1-2}r_3e^{-i2\delta_2}}$$

Now we have the Fresnel coefficient for the reflection of the entire graphene layer, which is the second layer in our stack, whose thickness is about 2 nm[9]. To achieve the full reflectivity of the cavity, we must include the air gap and the silicon subtrate as well, for which we formulate the following Fresnel coefficient in the same manner:

$$r_3 = \frac{r_{2-3} + r_{3-4}e^{-i2\delta_3}}{1 + r_{2-3}r_{3-4}e^{-i2\delta_3}} \tag{4.5}$$

We can now drop the double subscripts, and only take the initial indice. Substituting r_3 in $r_2(r_3)$ yields:

$$\begin{aligned} r_2 &= \frac{r_1 + [\frac{r_2+r_3e^{-i2\delta_3}}{1+r_2r_3e^{-i2\delta_3}}]e^{-i2\delta_2}}{1 + r_1[\frac{r_{2-3}+r_3e^{-i2\delta_3}}{1+r_2r_3e^{-i2\delta_3}}]e^{-i2\delta_2}} \\ &= \frac{(1+r_2r_3e^{-i2\delta_3})(r_1) + (r_2) + r_3e^{-i2\delta_3})e^{-i2\delta_2}}{(1+r_2r_3e^{-i2\delta_3}) + r_1(r_2 + r_3e^{-i2\delta_3})e^{-i2\delta_2}} \end{aligned}$$

With little algebra, this yields for $R_2 = r_2^2$, the reflectivity from the graphene, the following equation[11]:

$$R_2 = \left[\frac{r_1 + r_2e^{-i\delta_1} + r_3e^{-i(\delta_1+\delta_2)} + r_1r_2e^{-i(\delta_1+\delta_2)}}{1 + r_1r_2e^{-i\delta_1} + r_1r_3e^{-i\delta_2} + r_2r_3e^{-i\delta_2}}\right]^2$$

4.3.3. Fabry-Pérot interferometry

One of the working principles of the method is of course what is referred to as the nanomechanical resonator. That is the circular drum of graphene, suspended above a cavity of air below which only a reflective silicon substrate lies. Together, this peculiar combination of layers can together be regarded as a form of a Fabry-Pérot Cavity[2]. Such a cavity is an interferometric device, where incoming light is not fully transmitted but retained to some degree due partial reflection of the surfaces. The cavity is typically based on two opposing mirrors, which can transmit some light from external sources, and keep some of the light trapped in between. As one of our mirrors is the bilayer of graphene, the light is modulated because of interference, if the graphene moves up and down.

Recalling the depth of the cavity being 285 nm, the modulation of light due to graphene is visualised by the simulation in Figure 4.2. The simulation has been done on the found formula for the reflectivity of the graphene layer, R_2, and we later need this figure to find a conversion factor to deflection distance $z(t)$.

4.4. Equation for membrane deflection

The deflection z is the distance the membrane bulges up or down. For this measure, we take the distance the center of the membrane makes from its horizontal. Note that its natural position is somewhat down already, due to gravitational forces. The deflection, as used by Roslon et al.[9], is derived as follows.

First, it is assumed that the voltage obtained at the photodiode, V_{pd} is a function of time and hence also a function of deflection, z . Following

this, we note that this obtained voltage is related to the light intensity I by the reflectivity R of the surface, where this reflectivity is defined as $I_{in}(t)/I_0$, being the ratio of the laser intensity, I_0 and the perceived intensity $I_{in}(t)$ at the photodiode for each time t. This relation is assumed to be linear:

$$V_{pd} = \alpha\, R(z) I_0$$

Then, using this relation with the intensities,

Then we apply a Taylor's approximation, to get a first-order linear correction for R_0 to obtain $R(z)$:

$$R(z) = R_0 + \frac{d}{dz} R(z)|_{z_0}[z - z_0] = R_0[1 + \phi \Delta z] \quad (4.6)$$

Where we have defined ϕ as:

$$\phi = \frac{d}{dz}\left(\frac{R(z)}{R_0}\right) \quad (4.7)$$

This conversion factor can be obtained by running a simulation on the reflectivity R, and taking the slope as done in Figure 4.2. From this we find $\phi = -0.0038$.

We continue by assuming the mean voltage to be equal to the voltage obtained at the central position of the drum:

$$V_{pd}(g_0) = < V_{pd} >$$

Since we can find this mean value $< V_{pd} >$ from a datatrace, this is used in the final equation. This can be related as follows.

$$\frac{V_{pd}(z)}{< V_{pd} >} = \frac{R(z)}{R_0} = 1 + \phi \Delta z$$

By doing some algebra, we arrive at:

$$z(t) = \Delta z = \left[\frac{V_{pd}(z)}{< V_{pd} >} - 1\right] \phi^{-1} \quad (4.8)$$

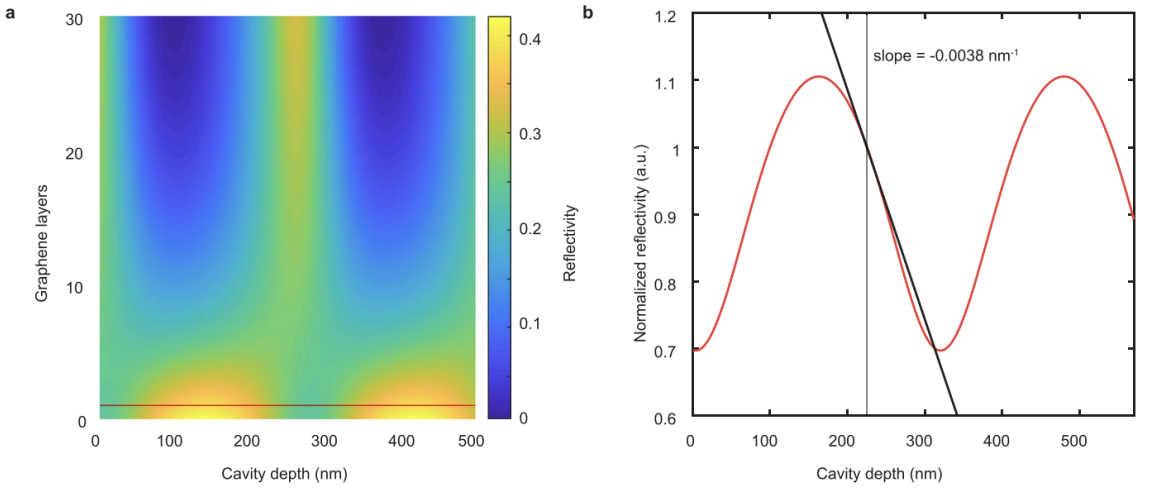

Figure 4.2: Figure adopted from Roslon et al. (2022), *Extended Data*[9] Original text belonging to the Figure: **Reflectivity of the Fabry-Pérot cavity formed by suspended graphene. a,** Reflectivity as a function of number of graphene layers and cavity depth. Values for bilayer graphene are indicated by a red line. **b,** The reflectivity change is normalized with respect to the natural position of the graphene drum. By determining the slope around this point, a sensitivity ϕ =−0.0038 nm^{-}1 is found.

5
Noise Analysis Framework

The further part of this paper will dive deeper into the amount of noise in comparable experiments by each of the two methods. Before doing so, the following paragraphs are aimed to elaborate some on the theory of noise sources and the relevant methods of analysis.

5.1. Variance as metric

When doing a series of tests or experiments, and the results are not as expected, it can be that the experiments are set up incorrectly, or noise is too prevalent, or a combination of both. One must always look very carefully in what is actually being measured, and from that basis, see what could be disturbing the signal of interest. For example, when recording a voice with other sounds in the distance, these other sounds become noise in the data; it is an unwanted constituent of the obtained signal that obstructs the analysis of the wanted signal.
There are multiple models for noise sources, and thus also multiple ways to quantify the amount of noise. For the research into nanomotion, the motility of cell is quantified by taking the variance of the signal, be it photodiode voltage or pixel intensity. Broadly speaking, the motion amplitude is deduced from the amount of spread in this original signal.
However, as has been noted earlier[9], the signal of an empty chip also has a certain amount of variance, of which the converted nanomotion yields deflections up to $2\,$nm. It is assumed that this is partly due to the underlying noise sources within the individual parts of the experimental set-up, and it is this reference level of noise that is the scope of this report.

Variance can be quantified using various methods, one of which involves calculating the mean squared deviation from the mean, represented by the equation:

$$\text{Var}(I) = \frac{1}{N}\sum_{i=0}^{N}(I(t) - < I >)^2 \qquad (5.1)$$

Where $I(t)$ represents individual data points, $< I >$ denotes the mean, and N is the total number of data points.

5.1.1. Power spectral density

Taking the Fourier transform of any obtained signal $V(t)$, and then taking the ensemble average of the magnitude of the transformed signal: $< |V^T|^2 > (f)$ [5], where f is the frequency, one can find a graph which represents the power, or weight, of the total signal as divided up up in different parts relating to a part of the frequency domain. In this sense, one can find the distribution of a signal over the frequencies. These type of plots are very powerful tools, one can find for example noise due to AC electronic interference (multiples of $50\,$Hz), the noise distribution ($1/f^a$ for pink noise, typical for living cells), white noise (nonliving signal). To use this type of analysis, it is good to have a longer signal and more datapoints, as both of these parameters put a limit on the frequencies which are included in a power spectral density.

5.1.2. Drift correction

It has been noted that the signals obtained using this method for nanomotion detection, can sometimes attain a linear drift[9]. This is possibly due to the warming of the components, by, for example the He-Ne laser. To compensate for the drift, a polynomial fit is taken and the linear growth is subtracted, to obtain a flat function.

5.2. Implementation of Parallel Readout

The method of Parallel Readout, being a new variant on the existing method, is not fully fixed and therefore some of the options chosen here do not fully represent the implementation of this method

yet. As said earlier, it is based on expanding the laser beam over a greater area, after which a CMOS Camera records a video from multiple cavities, which are to be analysed. The analysis that has been done here is similar to that of Single Spot Readout, as the center of each drum has been taken with a radius of $4\,\mu$m as the signal of interest. Each of the pixels within that $4\,\mu$m radius is averaged equally and taken as the data point for that instance. With 100 frames per second, we have 3000 points of data for each measurement.

5.3. Statistical criteria for comparison

To quantitatively compare the two methods, we need to find statistical criteria. The delay caused by failure of material in previous experiments, has made the search for a statistical criterion unconventional, as we will define criteria that are unofficial but are, for this research, still meaningful. In this paragraph we will define criteria for the distribution of the variance of deflection, σ_z^2 , which is assumed normally distributed and may have its parameters such as mean and variance differ from experiment to experiment. Since the parameter σ_z^2 is a stochastic quantity, it can be described with a variance (or deviation) and a mean as well. To avoid confusion, we use the following notation for the variance of the variance σ_z^2:

$$S^2 = \mathrm{Var}(\sigma_z^2)$$

And for the mean we speak of the quantity as μ . Subscripts either indicate the type of experiment: Air, LB, Hypermotile, Δ-MotAB, or it indicated the method used. For the definitions of criteria that follow here, generic subscripts for the experiment type is used: a and b .

5.3.1. Distance D between distributions

To describe a (unitless) measure for distance between the probability distributions of measurements between two types of experiments, we define the following:

$$D = \frac{|\mu_a - \mu_b|}{S_{\mathrm{tot}}} \tag{5.2}$$

Where the total standard deviation is added in a Pythagorean manner, by assumption that the two distributions are independent. This assumption is based on the fact that the measurements of different experiment types have had no influence on eachother. The total standard deviation is given as:

$$S_{tot} = \sqrt{S_a^2 + S_b^2} \tag{5.3}$$

The distance between the distributions of two experiments defined as D is already an interesting quantity on itself, however we can include a compensation for the number of samples N, by inserting the Standard Error into the equation for D. where the Standard Error is defined as:

$$S_{\mathrm{SE}} = \frac{S_a}{\sqrt{n}} \tag{5.4}$$

This then yields for D:

$$D_{\mathrm{SE}} = \frac{|\mu_a - \mu_b|}{S_{\mathrm{tot_{SE}}}} \tag{5.5}$$

Where

$$S_{\mathrm{tot_{SE}}} = \sqrt{{S_{\mathrm{SE_a}}}^2 + {S_{\mathrm{SE_b}}}^2} \tag{5.6}$$

To give some interpretation, we have defined D_{SE} as a measure for the distance between two distributions. We can see that when $D_{\mathrm{SE}} = 1$, the difference in mean values equals the standard error of the standard deviation of the distributions combined. From this interpretation, we want to use D_{SE} to determine whether two sets of measurements belong to different experiments. Specifically, whether we can discern experiments containing bacteria from those that contain pure noise, that is, the reference signal. For this, we somewhat arbitrarily set $D_{SE} > 5$ as the criterion to for a method to be able to discern bacterial signal from reference signal.

Also, in case $N_a = N_b = N$, the interesting property follows:

$$D_{\mathrm{SE}} = \sqrt{N} D \tag{5.7}$$

From this, we can find for a calculated D the number of samples required, N_{req} to reach this criterion.

6 Results

In this section we come to the main results that are used to compare single spot and parallel readout techniques.

6.1. Variance of measurements

Figures 6.1 and 6.2 show the results by the use of the method of single spot readout and parallel readout, respectively. The boxplot shows the median and spread of measured variance σ_z^2, which has been taken after each measurement's signal was converted to distance z. These results are from measurements taking 30 seconds by 4 types of experiments, divided in 3 different probing locations: "*On cavity*", "*Near cavity*" and "*Far from cavity*". These are discerned by the boxplot colour, as noted in the legend. The Y-axis of each plot divides the experiments up in the four types: Hypermotile, Δ-MotAB, LB and Air.

The boxplots have been made using the Python library *matplotlib* and give a sense of the distribution of the variable, in our case, σ_z^2. The boxplot shows the median of the set, by a black line, around which the interquartile range is given by a thick square. This interquartile range spans from the first quartile to the third quartile, covering the middle 50% of the data. The wiskers extend to the data which lies within 1.5 times the interquartile range, from the edges of the box. Data points outside this range are considered outliers and are plotted individually using circles. All previously mentioned statistical results such as median do not take these outliers into account.

From these two figures it follows that the reference noise levels are more strongly picked up in the method of single spot readout, whereas all these values have a lower mean and spread in the case of parallel readout. For both methods, there is no consistent difference between the location of probing.

To further quantify the differences between the methods, make use of the Table 6.1. Here, the results from four experiment types are presented, for both methods. All quantities are derived from the variance of deflection σ_z^2 , as described in Chapter 6. Noteworthy is the difference in sample mean, μ, between the two methods: 1.74 nm for single spot readout as compared to 0.31 nm in the case of parallel readout. On the other hand, for the experiment with the hypermotile cells, single spot readout scores lower with a mean value of 2.92 nm versus 5.95 nm for parallel readout.

6.2. Relating the distance criteria D within a method

In Table 6.2 the criterion for distance D has been calculated, comparing the signals of LB to that of the two types of bacteria for both parallel (beam) readout (PBR) and single spot readout (SSR). A higher value for D implies better distinction, and with a value of 2.35 for the distinction between LB vs. Hypermotile, parallel readout is more succesful than single spot readout on this area, as single spot readout has a distance D of 0.39. For the distinction between LB and the nonmotile Δ-MotAB there is no clear difference between the two methods.

With the use of the Standard Error, D_{SE} has been calculated for each situation and this gives a metric for distance between distributions corrected for the sample size N. By calculation methods as described in Chapter 9, the required sample size N_{req} has been found and put in the final column of Table 6.2. Here, it is clear that a bigger set of measurements is required for the distinction between nonmotile bacteria and a reference voltage to achieve the criterion of $D_{\mathrm{SE}} > 5$. By the method of parallel readout, this criterion has been achieved for distinguishing the reference signal obtained from pure LB from the signal obtained from hpermotile cells, value for D_{SE} of 9.40.

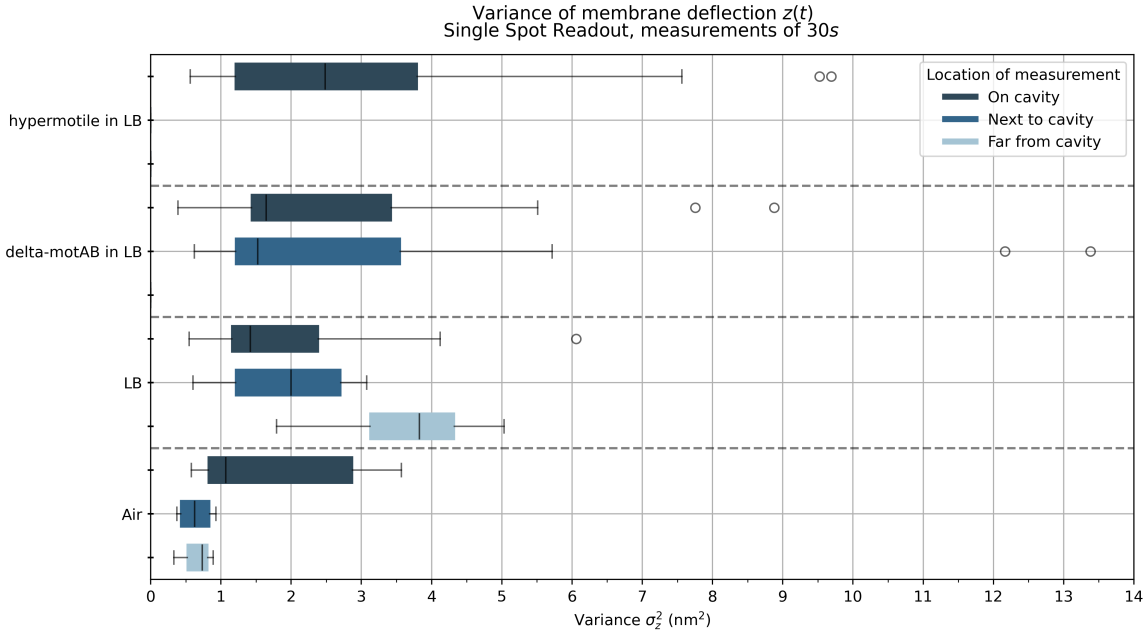

Figure 6.1: Boxplot containing the results from various experiments using Single Spot Readout. Note that no experiments have been conducted for the case Δ-MotAB, located far from cavity, as well for Hypermotile far from cavity and next to cavity. Sample sizes: for all cases "On Cavity", $n = 16$, except for Hypermotile, $n = 70$. For all cases "Next to cavity", $n = 8$, for all cases "Far from cavity", $n = 4$.

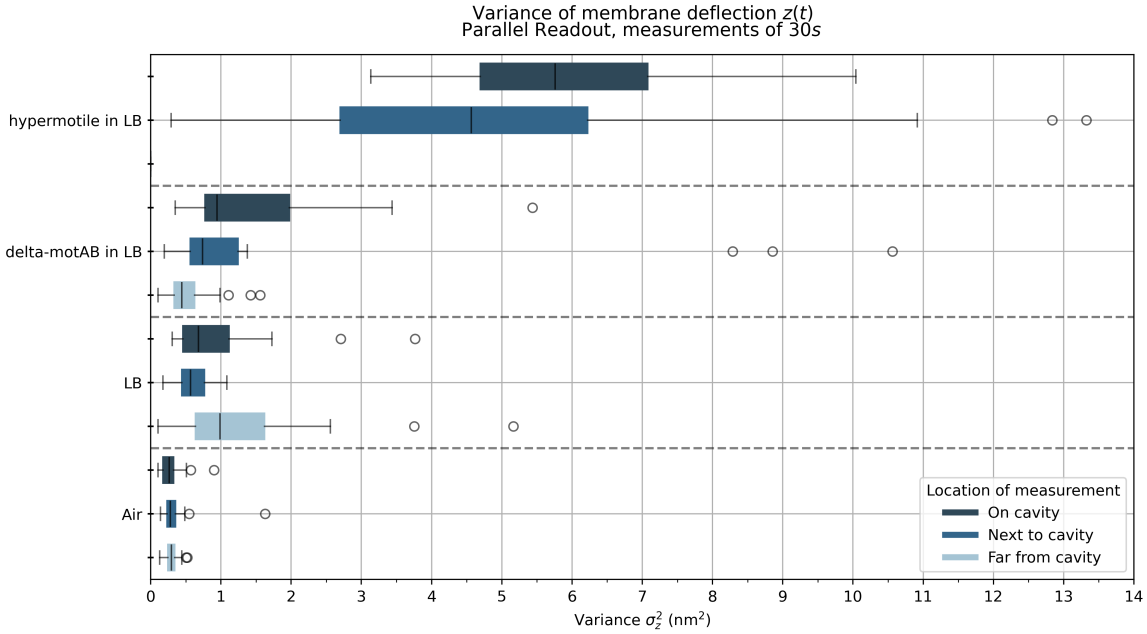

Figure 6.2: Boxplot containing the results from various experiments using Parallel Readout. Note that the experiment for the Hypermotile strain located far from cavity has not been conducted.
Sample sizes: for all cases "On Cavity", $n = 16$. For all cases "Next to cavity", $n = 20$, for all cases "Far from cavity", $n = 20$.

Table 6.1: Statistical results on the set of variances belonging to each experiment. Median values in this table can deviate somewhat from the medians as noted in the previously given boxplots, as here the outliers have been included in the calculations.
All values belong to experiments located "On Cavity".

Experiment	n [nm^2]	μ [nm^2]	S [nm^2]	Median [nm^2]	Standard Error $S_{\text{SE}} = \frac{S_a}{\sqrt{n}}$ [nm^2]
Single Spot Readout on Cavity					
Air	16	1.74	1.07	1.13	0.28
LB	16	1.95	1.42	1.38	0.35
Δ-MotAB	16	2.82	1.64	2.46	0.61
Hypermotile	70	2.92	2.48	2.06	0.25
Parallel Readout on Cavity					
Air	16	0.31	0.26	0.20	0.05
LB	16	1.03	0.68	0.92	0.23
Δ-MotAB	16	1.57	0.94	1.29	0.32
Hypermotile	16	5.95	5.76	1.88	0.47

Table 6.2: Results for the criteria as defined in Chapter 5 by which the two methods can be compared. The criteria are a measure for the amount in which one method obtains signals that have discernible characteristics for the reference signal versus a signal containing cells. N_{req} represents the number of samples required of an experiment in order to achieve the criterion $D_{\text{SE}} = 5$.
All values belong to experiments located "On Cavity".

Method	Comparison	$D = \frac{\lvert\mu_a - \mu_b\rvert}{S_{\text{tot}}}$	$D_{\text{SE}} = \frac{\lvert\mu_a - \mu_b\rvert}{S_{\text{tot}_{\text{SE}}}}$	$N_{\text{req}} = (5/D)^2$
PBR	LB vs. Δ-MotAB	0.34	1.34	216
PBR	LB vs. Hypermotile	2.35	9.40	4.5
SSR	LB vs. Δ-MotAB	0.31	1.24	260
SSR	LB vs. Hypermotile	0.39	2.10	164

7 Discussion

7.1. Distinction between the locations on the chip

The distinction between the three locations has been done to obtain a reference level of noise, but also to find the quality of the effect of the drums. From the results of these experiments, the variance of the signal coming from the drums is no stronger than from the other regions on the chip. From this it seems the signal, on average, has not been enhanced by the cavities, for these experiments.

7.2. Empty drums

From a manual inspection of the chip, for one experiment of both parallel readout and single spot readout containing cells, the membranes before and after were found 50% empty. This implies some part of the data gathered in these experiments with cells, does in fact not probe a cell and will yield the reference level of noise. One possible way to compensate for this, is to find a threshold on σ_z^2 for selecting measurements, and leave all signals that have a variance below that threshold out.

7.3. High variance of LB far from cavity

The experiments on pure LB were meant to obtain a reference level of noise, however it has not been expected that the region far from the cavities would contain more variance. This can be related to the flushing in of LB, of which the differences in pressure can cause motion of the fluid in all directions and make the signals more noisy.

7.4. Sampling frequency

The overall lower result in variance of the deflection in parallel readout in comparison to single spot readout, can be related to the sampling frequency of the two methods. For single spot readout, $f = 2000Hz$ while in the parallel case, $f = 100Hz$. This implies that higher frequency noise is more picked up in single spot readout, while that noise is averaged out in parallel readout.

7.5. Sample size and omitted experiments

The experiments as presented here have been done over due to previous difficulties with the breaking of drums on the chip from another manufacturer. This has put a time limit on the experiments, and hence the sample size is kept small.

8 Conclusion

This research is aimed at researching one of the challenges related to the implementation of parallel readout into a graphene-based bacterial motion detection technique. Specifically, the noise levels of parallel readout have been compared with the noise levels of the more established technique of single spot readout. Experiments have been have been conducted to quantify these levels of noise and the ability of both methods to discern between dead and living bacteria. As both methods obtain bacterial motility from the variance in its obtained signal, and this variance itself being distributed stochastically, we have sought for metrics quantifying the distance between the distributions of two experiments. With the use of unconventional metrics such as the distance between two distributions D_{SE}, as explained in Chapter 6, a comparison is finally made between the two techniques.

From this comparison, the method of parallel readout scores well on the highly motile bacteria. Specifically, for the criterion on distance between a signal and the reference signal we have set $D_{\mathsf{SE}} > 5$, and for highly motile bacteria, parallel readout scores $D_{\mathsf{SE}} = 9.40$, being the only case that has been performed that achieves this criterion. Thus the distinction between a living hypermotile cell and a reference signal can be made using this technique, and it can be concluded that the method of parallel readout is suitable for discerning hypermotile bacteria from non-bacterial samples. This can be extended to samples containing dead bacteria after application of antibiotics, making the method a powerful tool for susceptibility analysis. The power of this tool is in its capacity to be scaled up to probe a great amount of bacteria simultaneously.

During the research, a distinction has been made between three possible probing locations: being either "*On cavity*", "*Between cavities*" or "*Far from cavity*". However, no clear difference is noted in the signals obtained from these three different probing locations, which was expected. As the cavities act as Fabry-Pérot resonators, they modulate the incoming light when deflections of the membrane occur due to bacterial motion. Thus the obtained signal is expected to be different from the (non-modulated) direct reflection from the graphene, where the locations are not on top of the cavity. This calls for further understanding, and possibly research, into the effectiveness of the cavities in enhancing the signal. However, on this point it should be noted that the sample sizes of the experiments on locations away from the cavities are low ($n = 4$ or $n = 8$), weakening this recommendation.

The experiments where parallel readout was used have been conducted in a manner where four drums have been probed simultaneously, and further research needs to be done for scaling up this technique to more drums. One important problem that needs to be overcome is the proper handling of the high amount of data, which, after a few hours of measurement, can already amount up to hundreds of gigabytes if not compressed. The work in this paper can serve as a small step towards the implementation of parallel readout mechanisms in the use of probing bacteria, and interesting remarks follow in the next chapter, which could pose as future topics of research as well.

9 Outlook

During this research, for both methods multiple tools have been used in gaining an understanding of the buildup of the signal. The following text is meant as a summary of what has been found, and some of these are interesting points for future research.

9.1. Regarding Single Spot Readout

- **Comparison of individual signals** Figure 9.2 shows four signals obtained from the four types of experiments, all obtained from a focused laser aimed at a graphene drum. The difference between signals involving bacteria versus no bacteria is very noticeable, however between these two bacteria there is no clear difference. The hypermotile strain shows for this specific measurement only slightly higher variance, as indicated by σ^2 the text in the figure
- **Comparison of Power Spectral Densities** In Figure 9.1 a Power Spectral Density (PSD) is created from two measurements of two different experiments. The blue graph is from the measurement on pure air, and here the power is spread out more uniformly, which represents white noise. The signal from the bacterium has relatively more energy in the lower frequencies, reflecting the pink noise behaviour of bacteria. Since the measurements were done at a frequency of $2000\,\text{Hz}$, the x-axis is limited at $1000\,\text{Hz}$, in accordance with the Nyquist limit on sampling.
- **Electronic Noise** In the PSD given by Figure 9.1, peaks appear around multiples of $50Hz$. Electric noise can account for very noticeable effects on the data due to the systems high sensitivity.

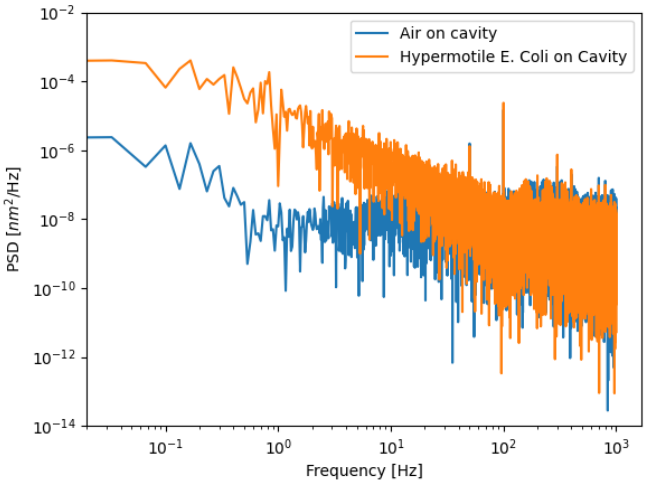

Figure 9.1: This figure shows the power spectral density calculated for two measurements of 30 seconds using Single Spot Readout. Calculations have been done using the SciPy package in Python.

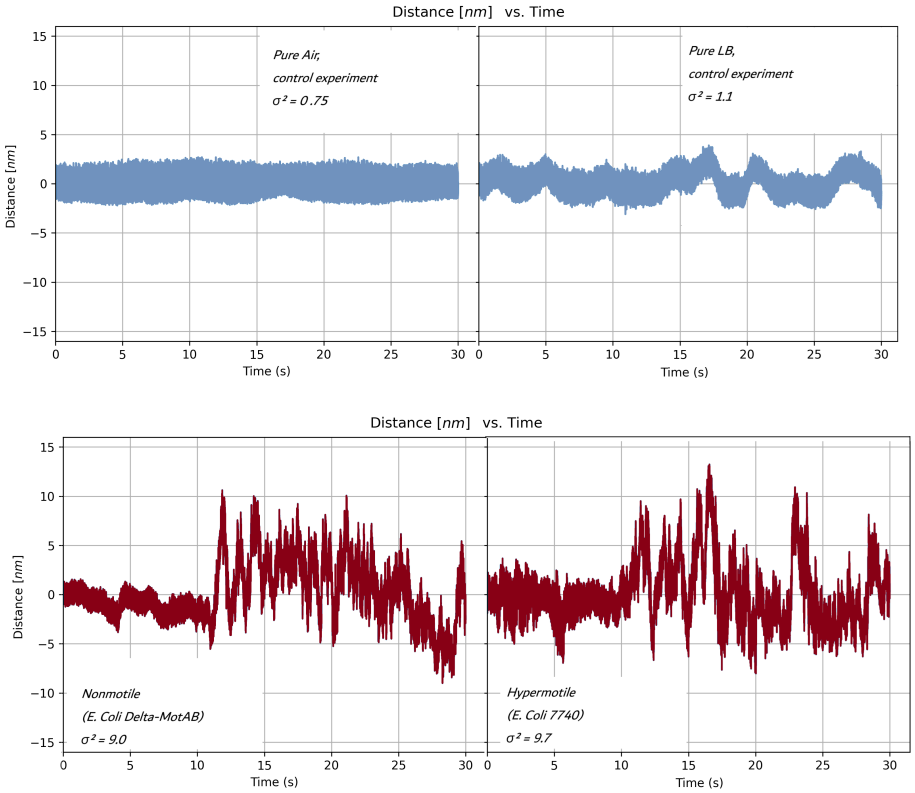

Figure 9.2: Figure containing four signals converted to membrane deflection in nanometer.

9.2. Regarding Parallel Readout

This section summarizes the insights on the signal obtained in parallel readout by the use of heatmaps. The heatmaps are either created using *ImageJ* or a script using Python and the *matplotlib* library. Either way, each pixel represents a value from a calculation of either the mean or the variance over the entire measurement. In that way, patterns occur which are not visible at first sight. It can even have future uses for bacterial motion research.

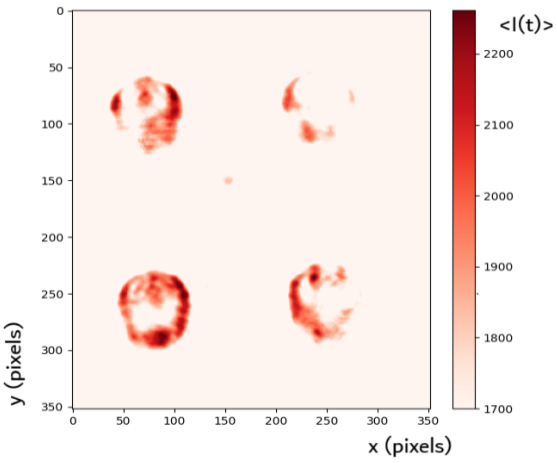

Figure 9.3: Heatmap of average pixel intensity over 30 seconds. Four cavities in pure air.

- **The cavities are the most reflective** Where the standard deviation heatmap can give insights into regions where the signal changes a lot, an average intensity heatmap can give interesting insights in, for example, where the most light is reflected. Figure 9.3 shows the average reflected intensity from the four cavities in air. The color scale is depicted to the right of it, and is a unitless number which ranges between 0 and 4096 (12 bit). By the adjustment of the scaling, only the cavities remain coloured, implying the highest reflection coming from the cavity surfaces.
- **Signals obtained in green and blue channels** From Figures 9.4 and 9.5, it is clear that light is gathered in the blue and green channels as well, even though the laser is purely red. The cause is not immediately clear, as an increase in photon energy is not expected - unless there

is some form of scattering. The signals can also be caused by errors in either the laser, which of course is not 100% monochromatic, or either the readout of the camera. Figure 9.4 shows the average intensity of one measurement of air on cavities, where only the blue channel is taken. Note that, here the cavities instead yield the least signal, in contrast to the red channel, where the cavities are brightest.

- **Fringe Patterns** Another puzzling remark from these heatmaps are the striped patterns that appear in 3 of the subfigures of Figure 9.5. It could be that these fringe patterns are related to the optical characteristics of the set-up. One option is due to self interference of the laser beam due to the widened angle in the expanded mode, which is necessary for parallel readout. As the laser is a highly coherent light source, different path lengths due to expansion can cause interference.
- **Observing bacterial motility** The bottom right part of Figure 9.5 shows a very interesting result. The variance of pixel intensity peaks at places where bacteria are deposited, and the image thus serves as a visualisation for the location and activity of bacteria. The image comes from a measurement where the nonmotile Δ-motAB E.Coli strain has been used, and succesfully sticked to the graphene using APTES. Four regions where bacterial movement can be seen are visible in the picture, and the size of each *splash* of color reflects the size of movements the bacterium undertakes.
- **Occurence of Hot Pixels** In Figure 9.4 also a few points are visible with intense brightness, much more than the surrounding. This is likely due to a phenomenon known as *hot pixels*, which occurs in CMOS devices when one of the pixel wells is responding too sensitive to incoming pixels.
- **Diffraction around the cavity** By inspection of the video material, sometimes rings around the cavities appear visible. Figure 9.6 a cavity in two modes. On the left, the drum is exposed to blue light, on the right it is exposed to the laser, and contrast has been increased of this right image to improve visibility of the fringes. The fringes do not only form around the cavity, but also run from a point which is off-center.

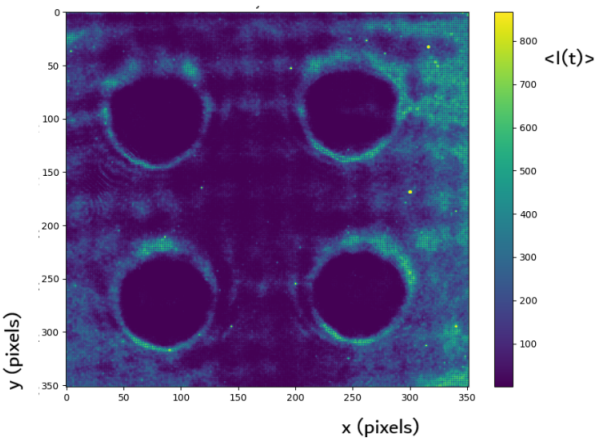

Figure 9.4: This image represents a heatmap of average intensity over one 30 second measurement of air.

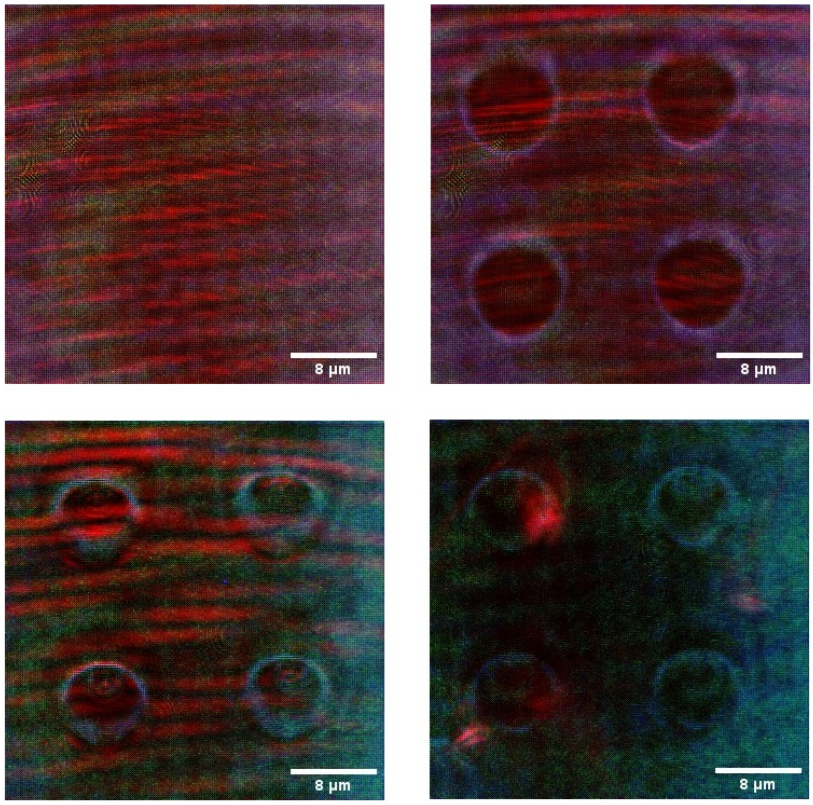

Figure 9.5: Heatmaps showing the standard deviation for each pixel over a measurement lasting 30 seconds. Each of the color channels shows their own standard deviation. The image is generated by performing a Z axis stack operation in *ImageJ*. The height of the Z-axis, being the standard deviations of pixel intensities, where not given but the image as it is does give room for quantitative analysis.
Going clockwise from the top left image: (1) measurement of pure air in a region far from the avities, (2) measurement of pure air over 4 cavities, (3) measurement of 4 cavities containing non-motile bacteria sticked with APTES, (4) measurement of 4 cavities on which pure LB is deposited.

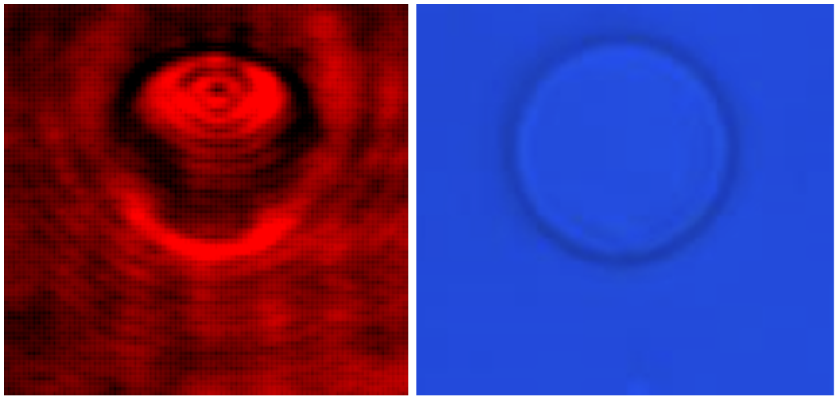

Figure 9.6: Image showing the diffraction effects in case the sample is lighted with He-Ne laser (left) and in case the regular blue light is used.

References

[1] D. Burnett. *The Science of Laboratory Diagnosis*. Wiley, 2005. ISBN: 978-0-470-85912-4.

[2] C. Fabry and A. Perot. “Theorie et applications d’une nouvelle methode de spectroscopie interferentielle”. In: *Ann. Chim. Phys.* 16.7 (1899). DOI: https://doi.org/10.1086/140557.

[3] A.K. Geim. “Graphene Prehistory”. In: *Physica Scripta* T146.2012 (2012). DOI: https://doi.org/10.1088/0031-8949/2012/T146/014003.

[4] Pierre Lecaruyer et al. “Generalization of the Rouard method to an absorbing thin-film stack and application to surface plasmon resonance”. In: *Applied Optics* 45.33 (2006).

[5] *Open Quantum Sensing and Measurement Notes*. https://qsm.quantumtinkerer.tudelft.nl/1_basics_of_noise/#12-power-spectral-density. Accessed: 5-2-2024.

[6] World Health Organization. *Global Action Plan on Antimicrobial Resistance*. 2005. ISBN: 978-92-4-150976-3. URL: https://iris.who.int/bitstream/handle/10665/193736/9789241509763_eng.pdf.

[7] Ferran Pujol-Vila, Rosa Villa, and Mar Alvarez. “Nanomechanical Sensors as a Tool for Bacteria Detection and Antibiotic Susceptibility Testing”. In: *Frontiers in Mechanical Engineering* 6 (2020), pp. 522–526. DOI: https://doi.org/10.3389/fmech.2020.00044.

[8] Irek E. Rosłoń et al. “Microwell-enhanced optical rapid antibiotic susceptibility testing of single bacteria”. In: *iScience* 26.11 (2023). DOI: https://doi.org/10.1016/j.isci.2023.108268.

[9] Irek E. Rosłoń et al. “Probing nanomotion of single bacteria with graphene drums”. In: *Nature Nanotech* 17 (2022), pp. 637–642. DOI: https://doi.org/10.1038/s41565-022-01111-6.

[10] Irek E. Rosłoń et al. “Prospects and challenges for graphene drums as sensors of individual bacteria”. In: *Applied Physics Letters* 124.1 (2023). DOI: https://doi.org/10.1063/5.0186160.

[11] M. P. Rouard. “Etudes des propriétés optiques des lames métalliques très minces”. In: *Ann. Phys. (Paris) Ser. II* 7 (1937), pp. 291–384.

[12] S. Mendoza Silva. *Identification of Bacteria with Articial Intelligence*. 2023.

[13] *User Manual, ThorCam Application Software*. https://www.thorlabs.com/drawings/c12e74540179d294-8B891644-EC64-A781-EC169F611EC10D39/CS235CU-SoftwareManual.pdf. Accessed: 30-1-2024.

[14] Antonin Vasicek. “Sur la réflexion de la lumière sur des verres supportant des couches minces multiples”. In: *Le Journal de Physique et le Radium* 11 (1990), p. 342.

[15] *What makes the Graphene Flagship: Graphene Flagship*. https://graphene-flagship.eu/about/our-story/. Accessed: 26-1-2024.